User interface tool for a novel plasma-assisted bio-additive extrusion system

Fengyuan Liu, Srichand Hinduja and Paulo Bártolo
School of Mechanical, Aerospace and Civil Engineering, University of Manchester, Manchester, UK

Abstract

Purpose – This paper aims to describe the control software of a novel manufacturing system called plasma-assisted bio-extrusion system (PABS), designed to produce complex multi-material and functionally graded scaffolds for tissue engineering applications. This fabrication system combines multiple pressure-assisted and screw-assisted printing heads and plasma jets. Control software allows the users to create single or multi-material constructs with uniform pore size or pore size gradients by changing the operation parameters, such as geometric parameters, lay-down pattern, filament distance, feed rate and layer thickness, and to produce functional graded scaffolds with different layer-by-layer coating/surface modification strategies by using the plasma modification system.

Design/methodology/approach – MATLAB GUI is used to develop the software, including the design of the user interface and the implementation of all mathematical programing for both multi-extrusion and plasma modification systems.

Findings – Based on the user definition, G programing codes are generated, enabling full integration and synchronization with the hardware of PABS. Single, multi-material and functionally graded scaffolds can be obtained by manipulating different materials, scaffold designs and processing parameters. The software is easy to use, allowing the efficient control of the PABS even for the fabrication of complex scaffolds.

Originality/value – This paper introduces a novel additive manufacturing system for tissue engineering applications describing in detail the software developed to control the system. This new fabrication system represents a step forward regarding the current state-of-the-art technology in the field of biomanufacturing, enabling the design and fabrication of more effective scaffolds matching the mechanical and surface characteristics of the surrounding tissue and enabling the incorporation of high number of cells uniformly distributed and the introduction of multiple cell types with positional specificity.

Keywords Scaffolds, Additive manufacturing, Multi-material printing, Control software

Paper type Research paper

1. Introduction

Additive manufacturing is a relatively new technology that creates three-dimensional (3D) structures joining material layer-by-layer (Gonzalez *et al.*, 2016; Gao *et al.*, 2015). This technology was developed during the 1980s as rapid prototyping processes, primarily for the fabrication of aesthetic models or for form and fit assessments. Developments in terms of materials and process optimization allowed the use of this technology for rapid tooling applications (direct or indirect fabrication of tools/molds) and rapid manufacturing of functional parts (Brooks and Brigden, 2016; Martinho *et al.*, 2009). Additive manufacturing processes are also being used together with topological optimization tools to produce complex-shape and light weight structures for automotive, aerospace and civil engineering applications (Joshi and Sheikh, 2015; Bos *et al.*, 2016). Depending on the applications, additive manufacturing has been used to process a wide range of materials such as metals, polymers, ceramics, composites and concrete (Pereira *et al.*, 2013a, 2013b; Gonçalves *et al.*, 2014; Frazier, 2014).

Additive manufacturing is also being explored for medical applications, to produce permanent metallic implants (e.g. titanium or stainless steel bone fixation implants), by using powder-bed fusion processes (electron beam melting or laser melting processes), hearing aids by using vat photo-polymerization techniques and scaffolds with or without cells for tissue engineering applications mainly using extrusion-based systems (Atzeni and Salmi, 2015; Melchels *et al.*, 2012).

Scaffolds are critical structures for tissue engineering applications. They act as physical substrates to allow cell adhesion, proliferation and differentiation, promoting the formation of a new tissue. They are produced using biocompatible and biodegradable materials (natural and synthetic polymers, ceramics and composites – Section 1.1)

The current issue and full text archive of this journal is available on Emerald Insight at: **www.emeraldinsight.com/1355-2546.htm**

Rapid Prototyping Journal
24/2 (2018) 368–378
Emerald Publishing Limited [ISSN 1355-2546]
[DOI 10.1108/RPJ-07-2016-0115]

Received 14 July 2016
Revised 1 March 2017
Accepted 16 March 2017

with specific level of porosity, pore shape, pore size, which depend on the tissue application, and pore interconnectivity.

1.1 Materials commonly used to produce biodegradable scaffolds

1 Synthetic polymers:
   - Poly(lactic acid), poly(glycolic acid), (lactic-co-glycolide) and poly(ε-caprolactone) (PCL).

2 Natural polymers:
   - Collagen, proteoglycans, alginate-based substrate and chitosan.

3 Ceramic materials:
   - Hydroxyapatite, β-tricalcium phosphate, calcium phosphates, magnesium phosphates and bioglasses.

Scaffolds must have a controlled degradation rate that must match the regeneration rate of new tissue, proper mechanical properties and surface characteristics (Almeida and Bartolo, 2014; Khoda *et al.*, 2011; Dhandayuthapani *et al.*, 2011).

Several systems were specifically developed to produce scaffolds for tissue engineering applications. Examples include machines being developed by RegenHU (Switzerland), Envisiontec (Switzerland), Organovo (USA), Cyfuse Biomedical (Japan), BioBots (USA), 3D Bioprinting Solutions (Russia), Rokit (South Korea) and Aspect Biosystems (Canada) (examples are provided in Figure 1). A significant number of these systems are limited to the fabrication of single-material scaffolds, which may not be fully chemically compatible with cells. For multi-material systems, most of the machines operate with multiple hydrogels (soft polymers), except Envisiontec, which allows to combine soft and hard materials. Moreover, available additive manufacturing processes are not able to produce scaffolds providing adequate chemical, physical and biological cues for cell growth in a tunable and effective way (Bártolo *et al.*, 2009; Pereira and Bártolo, 2015). As cells are sensitive to the surface characteristics of scaffolds (chemical and topographical properties), surface modification techniques such as cold plasma deposition, etching and grafting processes, can be used for tailoring the morphology and surface properties of scaffolds, thus improving and controlling the interactions with cells (Domingos *et al.*, 2013; Jacobs *et al.*, 2013). However, these treatments are performed in separated systems by increasing the fabrication time, manual handling and costs. This paper introduces a novel fabrication system to solve this problem. The system called plasma-assisted bio-extrusion system combines multiple printing heads and plasma jet operating with different gases to created multi-material scaffolds with controlled surface properties. The system requires a complex control software to manipulate different materials, scaffold designs and processing parameters. This software provides high design freedom, allowing to control geometric and process parameters such as lay-down pattern, filament distance, feed rate and layer thickness, as well as plasma-related parameter. The software developed to control the PABS system is described in detail in this paper, and examples illustrating the use of the software to produce different scaffolds are provided.

2. Plasma-assisted bio-extrusion system

PABS is a hybrid system (Figure 2) combining multi-extrusion and plasma jetting to process a great variety of biomaterials, from hydrogels (with or without cells) to hard-processed polymers and polymer composites. It enables to design and fabricate more effective scaffolds with specific surface properties (e.g. multi-material scaffolds with zonal regions containing different surface properties) and the incorporation of high number of cells, more uniformly distributed, and the introduction of multiple cell types with positional specificity. Table I shows the technical specification of PABS system.

The PABS hardware consists of two identical x-y plane linear motion systems and one z-axis build platform mounted on the same table, enabling multi-material dispensing and plasma modification in a sequential mode. Therefore, the plasma surface modification operation can be conducted either during or after the fabrication process, meaning that properties, such as chemical signaling, wettability, surface roughness and energy, can be modified in each layer at specific positions. The advantages of integrating the plasma process are the absence of solvents and the reduced amount of chemical reagents utilized and their intrinsic sterility due to the presence of highly energetic species (Khorasani *et al.*, 2008; Jacobs *et al.*, 2012; Cheng *et al.*, 2013; de Valence *et al.*, 2013).

3. User interface setup

3.1 User interface layout

The user interface was developed using MATLAB GUI, allowing users to design multi-material multi-pattern scaffolds with cylindrical and cubic shapes, automatically generating the corresponding G codes to control the machine. The layout of the user interface is shown in Figure 3. It comprises four main areas: scaffold definition, scaffold extrusion parameters setting, plasma parameter setting and scaffold lay-down pattern display:

1 *Scaffold definition area* [Figure 4(a)]: It allows the users to create single-material single-pattern scaffolds ("Single" option) and multi-material multi-pattern scaffolds ("Multiple" option). Primitives with different materials and lay-down patterns can be created separately and arranged in either vertical or horizontal direction.
2 *Extrusion parameters setting area* [Figure 4(b)]: This area allows the users to define processing parameters for the extrusion system, such as geometric parameters, position on the build platform, lay-down pattern, filament distance, feed rate, layer thickness and material. A solid or hollow scaffold structure can be filled with zigzag or parallel tool paths with set parameters.
3 *Plasma parameter setting area*: It allows the users to choose the processing gas and define the processing area for the plasma modification system, including geometric parameters, position on the build platform and feed rate. Lay-down pattern is all pre-defined in the programing part by filling the processing area with zigzag tool path.
4 *Display area*: Specified tool paths and lay-down patterns can be visualized in this area.

Once the users specify all geometric and process parameters, the boundaries of each primitive are determined, subroutines for the scanning tool paths generated and an output is saved in a text format. Figure 5 illustrates the structure of the program.

Figure 1 Examples of additive manufacturing systems specifically developed for tissue engineering applications

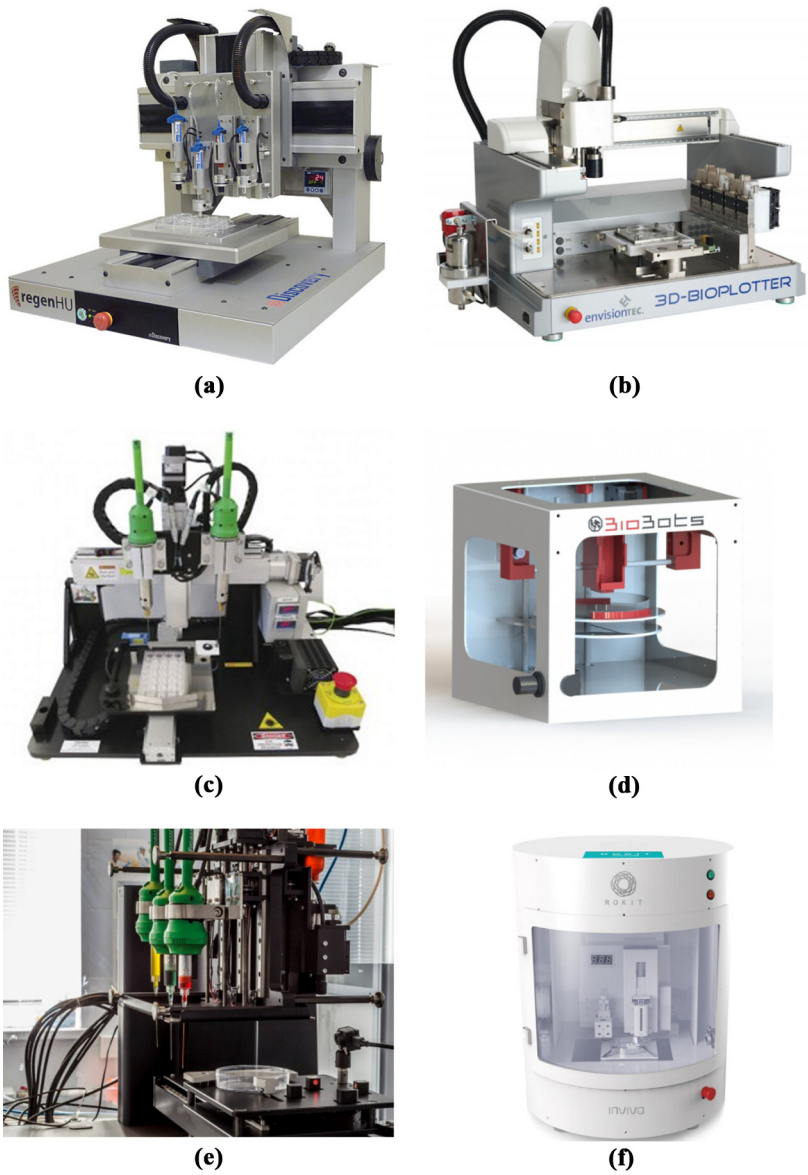

Notes: (a) 3D discovery from RegenHu; (b) 3D bioplotter from EnvisionTEC; (c) regenova from Cyfuse Biomedical; (d) biobots from Biobots Company; (e) 3dbio from 3D Printing Solutions Company; (f) edison Invivo 3D bioprinter from Rokit

3.2 Tool path generation

Two types of tool path are considered: zigzag and parallel (Figure 6). After the definition of the lay-down pattern parameters, the system automatically calculates the intersection points between a scanning line and the boundaries of a two-dimensional cross-section.

As illustrated in Figure 6, for a single material model, scanning lines P1-P4 and P5-P8 intersect the outer boundary at points P2, P3 and P6, P7. The tool path for a zigzag pattern is P2-P3-P7-P6. For a parallel pattern, the extrusion unit follows a scanning line P2-P3, and then the pressure turns off. After the building platform moves down and quickly travels to point P6, and the material deposition proceeds from P6 to P7.

For a horizontal multi-material scaffold, the inner primitives are printed in the sequence of "primitive no." by using the same algorithm as the single material scaffold before printing the outside part for each layer. As shown in Figure 7, after printing the filament for the tool path P1-P2-P3, a SKIP process is applied between P3 and P4. Afterwards, the external part is defined by printing from P4-P5.

The external part is printed as shown in Figure 8, which specifies the intersection points between scanning lines and the external boundary and all the nested loops. For each of the two

Figure 2 The front view of PABS system

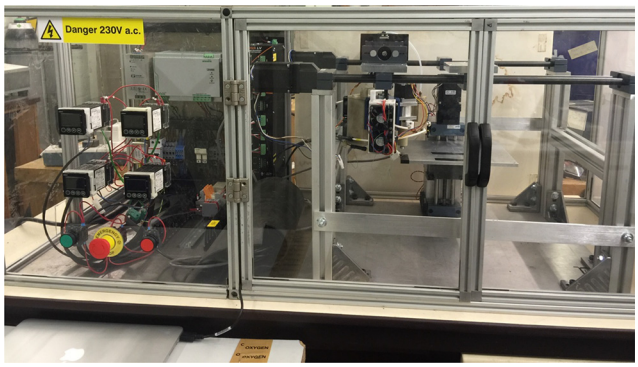

Table I Technical specifications of PABS system

Parameters	Working values
Working platform	A firm, even table, 250 × 200 × 7.5 mm
Material processing temperature	20-180°C
Humidity	10-90%, non-condensing
Electricity	Power supply 230 V AC, F 50/60 Hz
Air pressure	0-8 bar
Vibration	Stable working table is required
Deposition speed	0-20 mm/s
Screw rotational speed (only for the screw-assisted extrusion head)	0-20 rpm

Figure 3 Layout of the PABS user interface

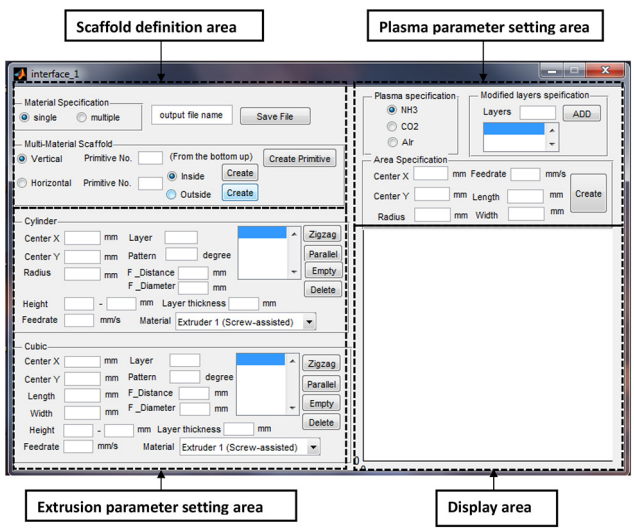

scanning lines shown in Figure 6, there are four intersection points, resulting in three segments. The rule is odd segments are retained and even segments are deleted, i.e. segments bounded by points P2-P3 are retained, whereas segments between P3-P4 are discarded. The printing sequences for the zigzag path [Figure 8(a)] and parallel path [Figure 8(b)] are different. For the zigzag path, the sequence is P2-P3-SKIP-P4-P5-P11-P10-SKIP-

Figure 4 Illustrations of the button functions for (a) scaffold type selection area and (b) scaffold parameters setting area

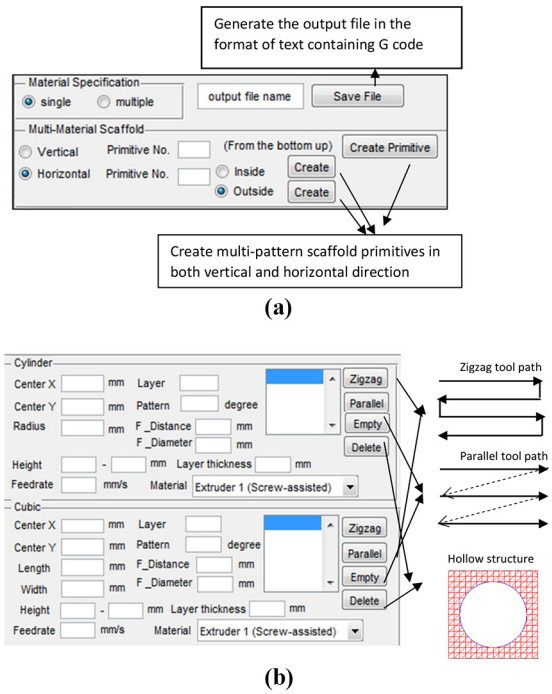

Figure 5 The PABS operation mode

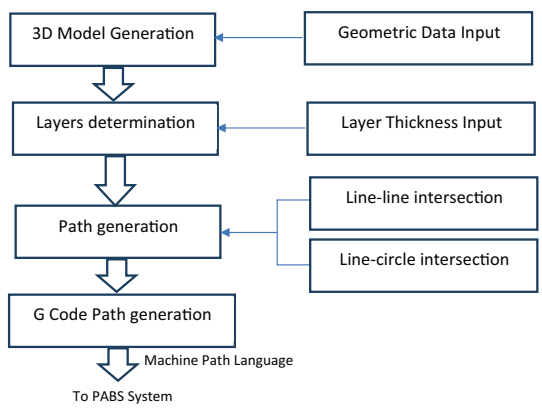

Figure 6 (a) Zigzag tool path pattern and (b) parallel tool path pattern for single material scaffold

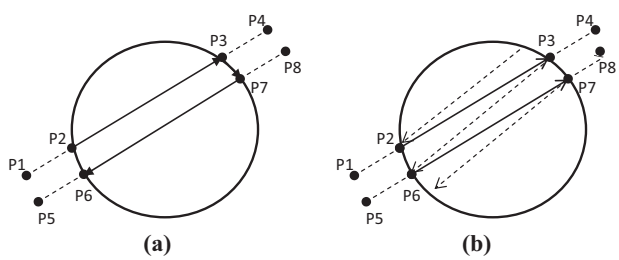

Figure 7 Tool path movements from the inner primitive to the outside primitive for horizontal multi-material scaffold

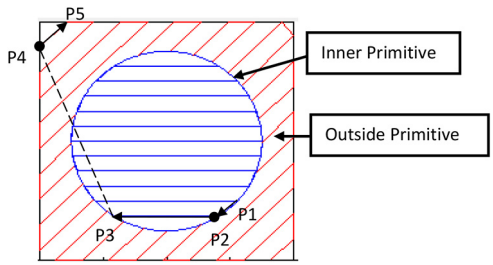

Figure 8 (a) Zigzag tool path and (b) parallel tool path for the outside part of horizontal gradient scaffold

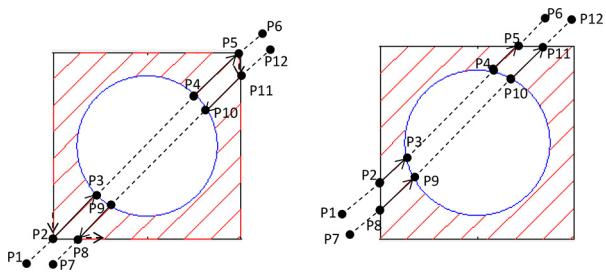

P9-P8, while for the parallel path, the sequence is P2-P3-SKIP-P4-P5-SKIP-P8-P9-SKIP-P10-P11. SKIP means that the extrusion units will switch off and deposit no material between two specific points. During this stage, the building platform moves down a safety distance (initial setting: 20 mm) and moves back when the extrusion unit reaches the new starting point. Figure 9 shows the front cross-section view of the SKIP process.

A similar algorithm is used for a vertical multi-material scaffold. The only difference is that parameters such as material type, scaffold architecture and shape can change along the vertical direction.

3.3 Nozzle diameter offset

When the extrusion unit deposits new materials intersecting with previous printed ones [Figure 10 (a)], the offset of filament diameter needs to be considered to avoid material overlapping. As illustrated in Figure 10(b), both the arc CD (diameter = D) and the inner tool path EF belong to the Inner primitive I, and the outside tool path AB belongs to the Outside primitive Π. The filament diameters for the Inner primitive I and Outside primitive Π are *d1* and *d2*. The algorithm for printing at the intersect section comprises the following steps:

- First, the circle contour is deposited along CD with filament diameter d_1.
- The intersect point between the inner tool path EF and the contour CD can be calculated using line-circle intersection algorithm, whereas the circle diameter requires an offset, which is $(D - 2d_1)$ along arc C"D", as shown in Figure 10(b). The intersection point is E.
- The intersect point between the outside tool path AB and the contour CD can be calculated using the line-circle intersection algorithm, whereas the circle diameter requires an offset, which is $[D+(d_1 + d_2)]$ along arc C'D', as shown in Figure 10(b). The intersection point is B.

Figure 9 Front cross-section view of the SKIP process

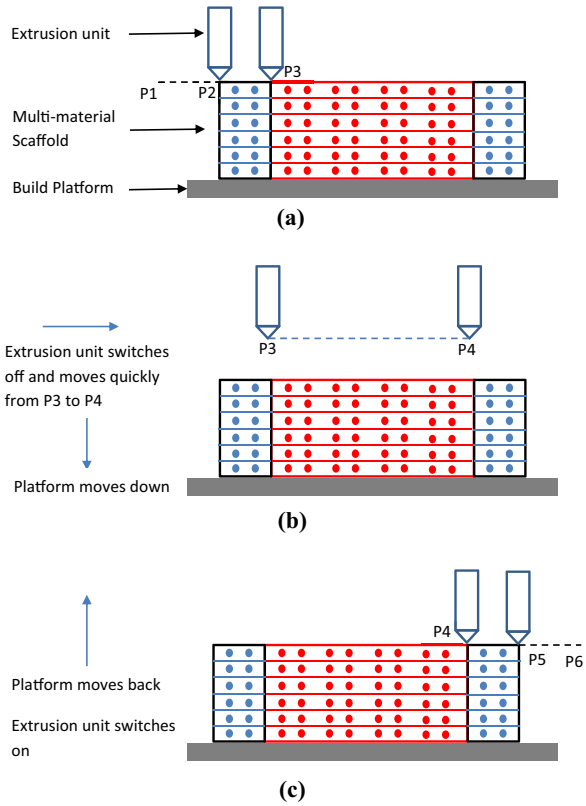

Notes: (a) Extrusion head deposits the outside part from P2 to P3; (b) build plat-form moves down, extrusion head switches off and moves quickly from P3 to P4; (c) the build platform moves back, extrusion head switches on and deposition continues from P4 to P5

Figure 10 Nozzle diameter offset at the intersection point

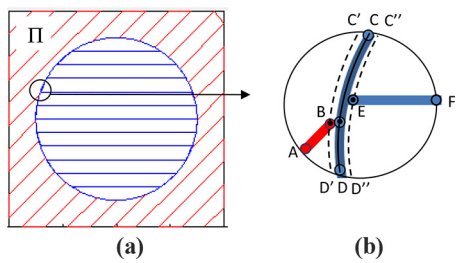

3.4 Material selection

Figure 11 schematically represents the extrusion unit, which is driven by a stepper motor. It comprises three extruders, located with the same interval of 120°. Depending on the material selection, the corresponding extruder rotates to be positioned at the printing position. Extruder 1 is set to be in the starting position with an angle of 0°. Depending on the materials being printed, the extruder movements are:

- *Extruder 1*: Extruder unit rotates to the set position of angle 0°.

Figure 11 Schematic of the multi-extrusion unit inter-change movement

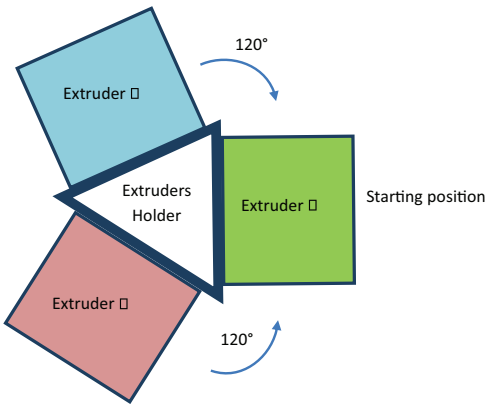

Figure 12 Schematic of the multi-jet plasma unit

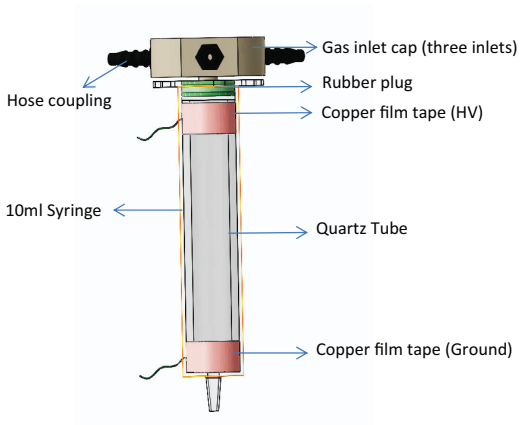

- *Extruder 2*: Extruder unit rotates to the set position of angle 0°, and counter-clockwise 120° to the starting position.
- *Extruder 3*: Extruder unit rotates to the set position of angle 0°, and clockwise 120° to the starting position.

This rotational system containing two pressure-assisted extruders and one screw-assisted extruder is unique. The screw-assisted head is based on one of the author's patent, which is now being used by Regenhu (Almeida *et al.*, 2010).

3.5 Plasma jet gas selection and tool path offset

The plasma unit comprises an atmospheric plasma jet system with three gas (air, NH_3 and CO_2) inlets mounted to the X-Y moving system. Figure 12 shows the schematic set up of the plasma jet. The selection of the gas is controlled using a gas solenoid valve so that users can change the processing gas manually. This design of the plasma jet also allows for the mixture of different gases.

The plasma will be generated between the high voltage (HV) copper film and the ground copper film, expanding to the surrounding air outside the nozzle. The diameter of the plasma jet will be varied by changing the supplied voltage and the flow of the gas. To achieve a comprehensive surface treatment in the specific area, the offset of the plasma jet diameter is defined using the same strategies, as explained in Section 3.3.

4. Deposition principle and algorithms

The software was developed to allow users to create scaffolds with external or internal circular or cubic geometries. Therefore, two types of intersections can be considered: line-line and line-circle intersections. This section describes the procedure for calculating these intersection points.

4.1 Line-line intersection

Consider two lines identified as Line a and Line b. Line a is defined by P1 and P2, and line b by P3 and P4; μ_a and μ_b are parametric co-ordinates varying from 0 to 1. These two lines can be written in parametric forms as follows:

Figure 13 Representation of different positions of two generic lines in the same space

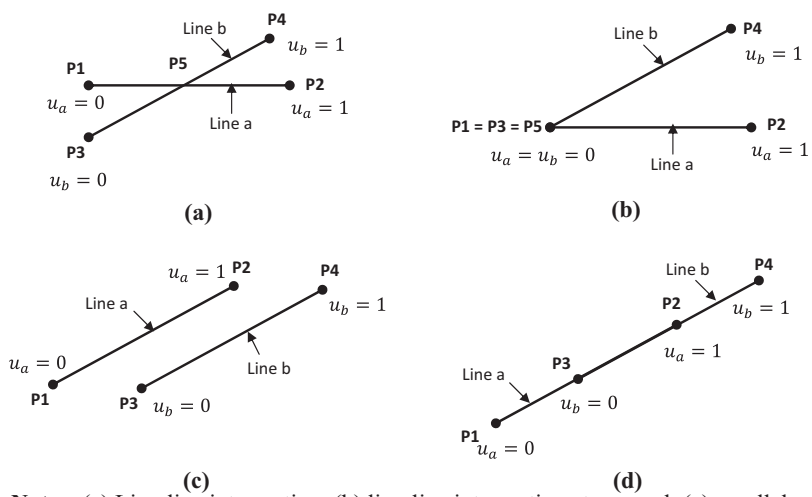

Notes: (a) Line-line intersection; (b) line-line intersection at one end; (c) parallel lines; (d) overlap lines

$$\overline{P}_a = \overline{P}_1 + u_a(\overline{P}_2 - \overline{P}_1) \quad (1)$$

$$\overline{P}_b = \overline{P}_3 + u_b(\overline{P}_3 - \overline{P}_4) \quad (2)$$

As the intersection point of the two lines has the same x, y coordinates, i.e. $P_a = P_b$, equations (1) and (2) can be transformed into:

$$x_1 + u_a(x_2 - x_1) = x_3 + u_b(x_4 - x_3) \quad (3)$$

$$y_1 + u_a(y_2 - y_1) = y_3 + u_b(y_4 - y_3) \quad (4)$$

The two unknown parametric co-ordinates u_a and u_b can be calculated by solving equations (3) and (4):

$$u_a = \frac{(x_4 - x_3)(y_1 - y_3) - (y_4 - y_3)(x_1 - x_3)}{(y_4 - y_3)(x_2 - x_1) - (x_4 - x)(y_2 - y_1)} \quad (5)$$

$$u_b = \frac{(x_2 - x_1)(y_1 - y_3) - (y_2 - y_1)(x_1 - x_3)}{(y_4 - y_3)(x_2 - x_1) - (x_4 - x)(y_2 - y_1)} \quad (6)$$

The values of u_a and u_b are used to check whether line vectors are intersecting the line entity. If $0 \leq u_a \leq 1$ and $0 \leq u_b \leq 1$, the intersection point between the two lines is valid [Figure 13(a)]. If $u_a = 1$ and $u_b = 0$, or vice versa, or $u_a = 1$ and $u_b = 1$, or $u_a = 0$ and $u_b = 0$, then the intersection point is one common end point of the two lines [Figure 13(b)]. According to equations (5) and (6), the two lines are parallel when the denominators for both equations are zero [Figure 13(c)], and overlap if both denominator and numerator are zero [Figure 13(d)].

Figure 14 Relative positions between a line and a circle in the same space

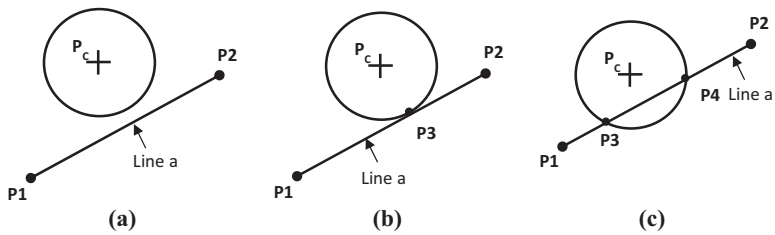

Notes: (a) No intersection; (b) line tangent to the circle; (c) line intersecting the circle at two points

Figure 15 Flowcharts for single-material scaffolds with/without plasma modification

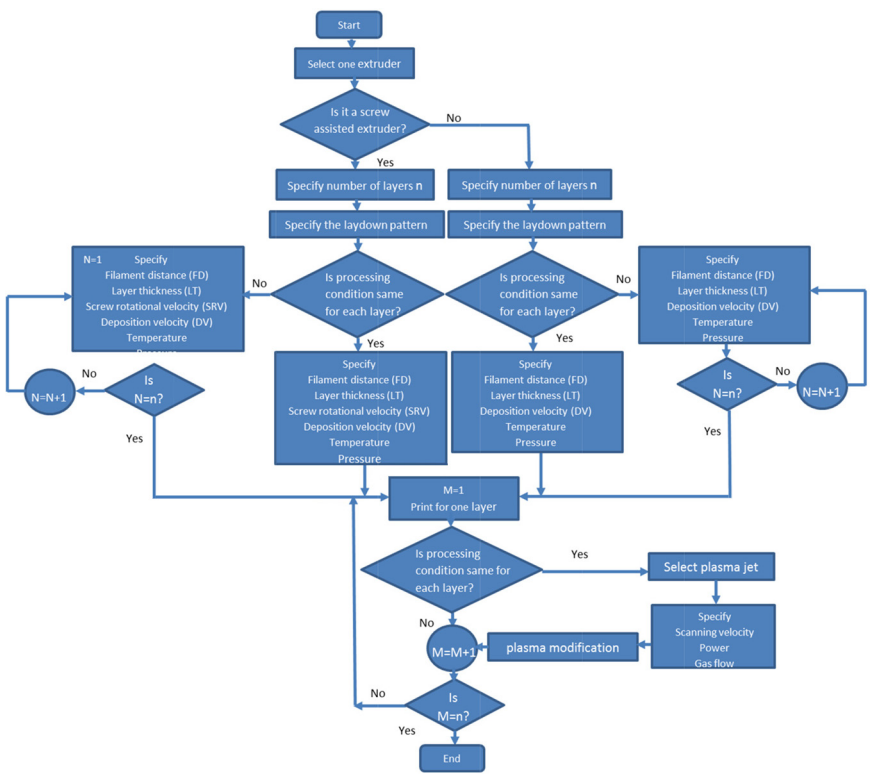

Figure 16 Flowcharts for multi-material scaffolds with/without plasma modification

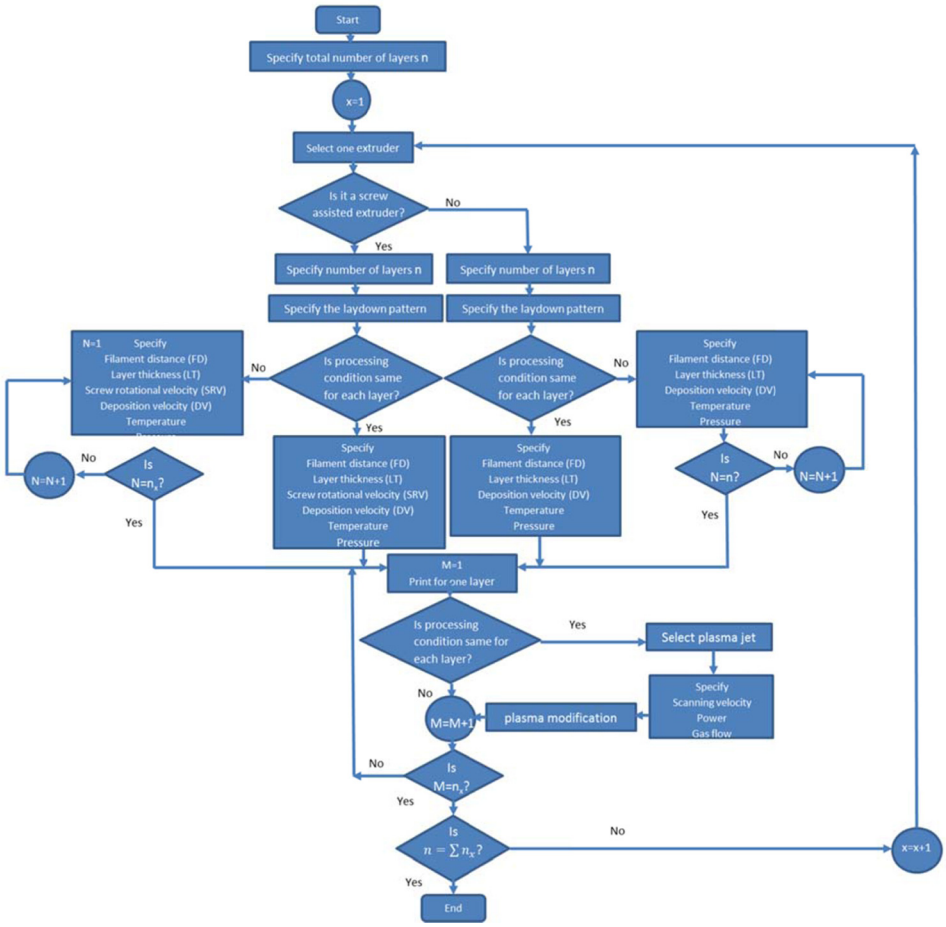

The coordinates of the intersection point P5 can be calculated by substituting equation (5) [or equation (6)] into equation (1) [or equation (2)], according to the following equations:

$$x_5 = x_1 + u_a(x_2 - x_1) \tag{7}$$

$$y_5 = y_1 + u_a(y_2 - y_1) \tag{8}$$

4.2 Line-circle intersection

There are three conditions for the intersection between a line and a circle: no intersection point; intersection at one point; and intersection at two points (Figure 14).

The equation for a circle entity centered at P_C (x_c, y_c) with radius r is given by:

$$(x - x_c)^2 + (y - y_c)^2 = r^2 \tag{9}$$

In the case of intersection at two points, $P_3(x_3, y_3)$ and $P_4(x_4, y_4)$ [Figure 14(c)], the equations for the intersection points coordinates can be derived from equation (1) as follows:

$$x = x_1 + u_a(x_2 - x_1) \tag{10}$$

$$y = y_1 + u_a(y_2 - y_1) \tag{11}$$

Substituting equations (10) and (11) into equation (9), a quadratic equation can be derived:

$$a \cdot u^2 + b \cdot u^2 + c = 0 \tag{12}$$

where:

$$a = (x_2 - x_1)^2 + (y_2 - y_1)^2 \tag{13}$$

$$b = 2\left[(x_2 - x_1)(x_1 - x_c) + (y_2 - y_1)(y_1 - y_c)\right] \tag{14}$$

$$c = x_1^{\,2} + x_c^{\,2} + y_1^{\,2} + y_c^{\,2} - 2(x_1 x_c + y_1 y_c) - r^2 \tag{15}$$

The solution to this quadratic equation is given by:

$$u_{3,4} = \frac{-b \pm \sqrt{S}}{2 \cdot a} \tag{16}$$

where $S = b^2 - 4 \cdot a \cdot c$

If $S < 0$, then the line does not intersect the circle [Figure 14(a)]. If $S = 0$, the line P_1P_2 is tangent to the circle and intersects it at one point [Figure 14(b)], where $u_3 = -b/2a$. The coordinates of the intersection point P_3 is given by:

Figure 17 Examples of different scaffolds configurations

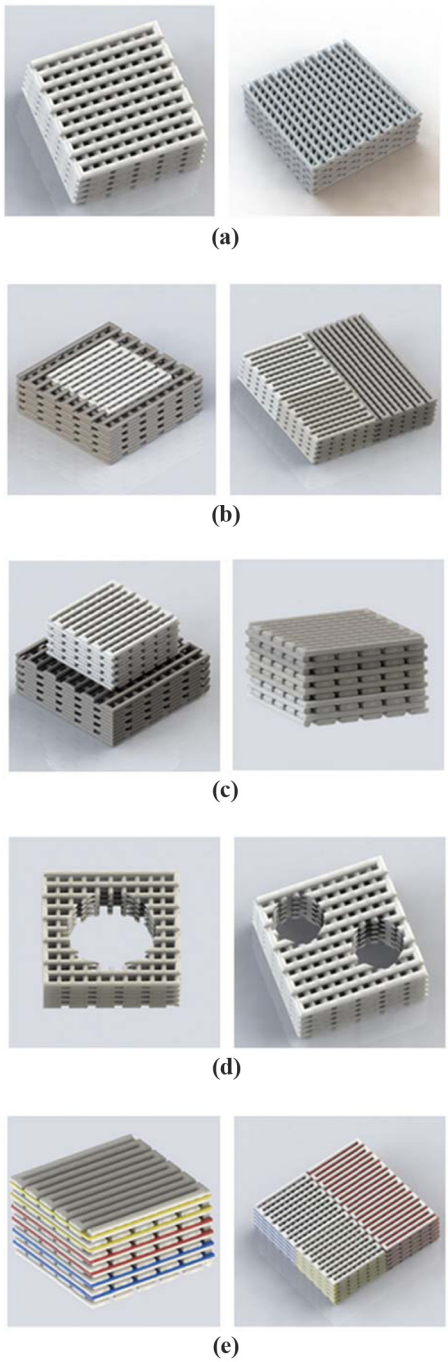

Notes: (a) Single-material single-pattern scaffold; (b) multi-material horizontal pattering scaffold; (c) multi-material vertical patterning scaffold; (d) hollow scaffold; (e) vertical/horizontal patterning plasma modified scaffolds

$$x_3 = x_1 + u_3(x_2 - x_1) \tag{17}$$

$$y_3 = y_1 + u_3(y_2 - y_1) \tag{18}$$

If $S > 0$, the line intersects the circle at two points P_3 and P_4.

$$x_4 = x_1 + u_4(x_2 - x_1) \tag{19}$$

$$y_4 = y_1 + u_4(y_2 - y_1) \tag{20}$$

4.3 Fabrication flowchart

Figures 15 and 16 describe the flowchart information required to produce scaffolds with different geometric parameters, lay-down pattern, filament distance, feed rate, layer thickness and plasma parameters. From these figures, it is possible to observe that the PABS system can be used to produce two main types of scaffolds:

1 single-material scaffolds with/without plasma modification (Figure 15); and
2 multi-material scaffolds with/without plasma modification (Figure 16).

5. Examples

The control software previously described gives high flexibility in terms of geometries to be build and material combinations. Single-material single-pattern scaffolds are the simplest and widely used type of scaffolds. The geometric shapes can be cylinder and cubic structures with user-defined dimensions. Figure 17(a) illustrates examples of a single-material scaffolds produced with 0°-90° and 0°-45°-90° laydown patterns. Other possible configurations include multi-material horizontal patterning scaffolds [Figure 17(b)], containing several sections of different materials, lay-down patterns or geometric shapes in x-y plane; multi-material vertical patterning scaffolds [Figure 17(c)], containing different subsections of different materials, laydown pattern or geometric shapes in the vertical direction; and hollow holes inside both single-material scaffolds [Figure 17(d)] and vertical/horizontal patterning multi-plasma modified scaffolds [Figure 17(e)]. Examples of produced scaffolds are presented in Figure 18.

6. Conclusions

The PABS's control software described in this paper provides high freedom of design, allowing the users to create single or multi-material constructs with uniform pore size or pore size gradients by changing process parameters, such as lay-down pattern, filament distance, feed rate and layer thickness. Functionally graded scaffolds can be designed considering different layer-by-layer coating/surface modification strategies by using the jet plasma system. Based on the user definition, G programing codes are generated, enabling full integration and synchronization with the hardware of the PABS system.

Figure 18 Examples of printed scaffolds by using PABS

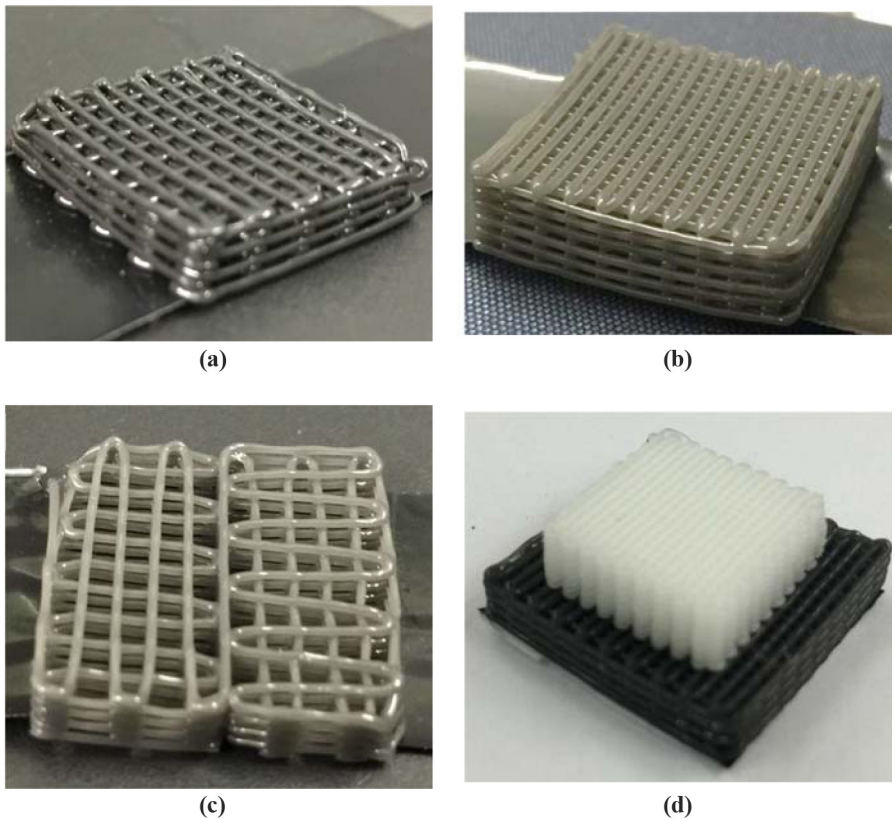

Notes: (a) PCL/carbon nanotube (CNT; 5 Wt.% of CNTs) single patterning (0.5 mm filament diameter; 1.5 mm filament distance; 4 mm height; 110°C melting temperature; deposition speed: 2.6 mm/s; screw rotational speed: 15 rpm) scaffold; (b) PCL/CNT (2.5 Wt.% of CNTs) single patterning (0.5 mm filament diameter; 0.5 mm filament distance; 6 mm height; 110°C melting temperature; deposition speed: 3 mm/s; screw rotational speed: 15 rpm) scaffold; (c) horizontal patterning scaffold with same material (PCL/CNT (1 Wt.% of CNTs) using different deposition strategies (left scaffold: 0/90° depositing direction; right scaffold: 90/0° depositing direction); (d) vertical patterning scaffold with different materials [upper scaffold: PCL; lower scaffold: PCL/CNT (5 per cent)] obtained using different depositing strategies (upper scaffold: 0.33 mm filament diameter and 0.4 mm filament distance; lower scaffold: 0.5 mm filament diameter and 0.5 mm filament distance)

References

Almeida, H.A. and Bartolo, P.J. (2014), "Design of tissue engineering scaffolds based on hyperbolic surfaces: structural numerical evaluation", *Medical Engineering & Physics*, Vol. 36 No. 8, pp. 1033-1040.

Almeida, H.A., Bartolo, P.J., Mota, C.M. and Mateus, A.J. (2010), "Processo e equipamento de fabrico rápido por bioextrusão", Portuguese Patent PT104247B.

Atzeni, E. and Salmi, A. (2015), "Evaluation of additive manufacturing (AM) techniques for the production of metal-ceramic dental restorations", *Journal of Manufacturing Processes*, Vol. 20 No. P1, pp. 40-45.

Bártolo, P.J., Chua, C.K., Almeida, H.A., Chou, S.M. and Lim, A.S.C. (2009), "Biomanufacturing for tissue engineering: present and future trends", *Virtual and Physical Prototyping*, Vol. 4 No. 4, pp. 203-216.

Bos, F., Wolfs, R., Ahmed, Z. and Salet, T. (2016), "Additive manufacturing of concrete in construction: potentials and challenges of 3D concrete printing", *Virtual and Physical Prototyping*, Vol. 11 No. 3, pp. 209-225.

Brooks, H. and Brigden, K. (2016), "Design of conformal cooling layers with self-supporting lattices for additive manufacturing tooling", *Additive Manufacturing*, Vol. 11 No. 3, pp. 16-22.

Cheng, Q., Lee, B.L.P., Komvopoulos, K., Yan, Z. and Li, S. (2013), "Plasma surface chemical treatment of electrospun poly (L-lactide) microfibrous scaffolds for enhanced cell adhesion, growth, and infiltration", *Tissue Engineering Part A*, Vol. 19 Nos 9/10, pp. 1188-1198.

de Valence, S., Tille, J.C., Chaabane, C., Gurny, R., Bochaton-Piallat, M.L., Walpoth, B.H. and Möller, M. (2013), "Plasma treatment for improving cell biocompatibility of a biodegradable polymer scaffold for vascular graft applications", *European*

Journal of Pharmaceutics and Biopharmaceutics, Vol. 85 No. 1, pp. 78-86.

Dhandayuthapani, B., Yoshida, Y., Maekawa, T. and Kumar, D.S. (2011), "Polymeric scaffolds in tissue engineering application: a review", *International Journal of Polymer Science, Article ID 290602*, Vol. 2011.

Domingos, M., Intranuovo, F., Gloria, A., Gristina, R., Ambrosio, L., Bártolo, P.J. and Favia, P. (2013), "Improved osteoblast cell affinity on plasma-modified 3-D extruded PCL scaffolds", *Acta Biomaterialia*, Vol. 9 No. 4, pp. 5997-6005.

Frazier, W.E. (2014), "Metal additive manufacturing: a review", *Journal of Materials Engineering and Performance*, Vol. 23 No. 6, pp. 1917-1928.

Gao, W., Zhang, Y., Ramanujan, D., Ramani, K., Chen, Y., Williams, C.B., Wang, C.C., Shin, Y.C., Zhang, S. and Zavattieri, P.D. (2015), "The status, challenges, and future of additive manufacturing in engineering", *Computer-Aided Design*, Vol. 69 No. 4, pp. 65-89.

Gonçalves, F.A., Costa, C.S., Fabela, I.G., Farinha, D., Faneca, H., Simões, P.N., Serra, A.C., Bártolo, P.J. and Coelho, J.F. (2014), "3D printing of new biobased unsaturated polyesters by microstereo-thermal-lithography", *Biofabrication*, Vol. 6 No. 3, p.- 035024.

Gonzalez, J.A., Mireles, J., Lin, Y. and Wicker, R.B. (2016), "Characterization of ceramic components fabricated using binder jetting additive manufacturing technology", *Ceramics International*, Vol. 42 No. 9, pp. 10559-10564.

Jacobs, T., Declercq, H., De Geyter, N., Cornelissen, R., Dubruel, P., Leys, C. and Morent, R. (2013), "Improved cell adhesion to flat and porous plasma-treated poly-ε-caprolactone samples", *Surface and Coatings Technology*, Vol. 232, pp. 447-455.

Jacobs, T., Morent, R., De Geyter, N., Dubruel, P. and Leys, C. (2012), "Plasma surface modification of biomedical polymers: influence on cell-material interaction", *Plasma Chemistry and Plasma Processing*, Vol. 32 No. 5, pp. 1039-1073.

Joshi, S.C. and Sheikh, A.A. (2015), "3D printing in aerospace and its long-term sustainability", *Virtual and Physical Prototyping*, Vol. 10 No. 4, pp. 175-185.

Khoda, A.K.M., Ozbolat, I.T. and Koc, B. (2011), "A functionally gradient variational porosity architecture for hollowed scaffolds fabrication", *Biofabrication*, Vol. 3 No. 3, p. 034106.

Khorasani, M.T., Mirzadeh, H. and Irani, S. (2008), "Plasma surface modification of poly (L-lactic acid) and poly (lactic-co-glycolic acid) films for improvement of nerve cells adhesion", *Radiation Physics and Chemistry*, Vol. 77 No. 3, pp. 280-287.

Martinho, P., Bartolo, P.J. and Pouzada, A.S. (2009), "Hybrid moulds: effect of the moulding blocks on the morphology and dimensional properties", *Rapid Prototyping Journal*, Vol. 15 No. 1, pp. 71-82.

Melchels, F.P.W., Domingos, M.A.N., Klein, T.J., Malda, J., Bártolo, P.J. and Hutmacher, D.W. (2012), "Additive manufacturing of tissues and organs", *Progress in Polymer Science*, Vol. 37 No. 8, pp. 1079-1104.

Pereira, R.F. and Bártolo, P.J. (2015), "3D photo-fabrication for tissue engineering and drug delivery", *Engineering*, Vol. 1 No. 1, pp. 90-112.

Pereira, R.F., Barrias, C.C., Granja, P.L. and Bartolo, P.J. (2013a), "Advanced biofabrication strategies for skin regeneration and repair", *Nanomedicine*, Vol. 8 No. 4, pp. 603-621.

Pereira, R.F., Carvalho, A., Gil, M.H., Mendes, A. and Bártolo, P.J. (2013b), "Influence of aloe vera on water absorption and enzymatic in vitro degradation of alginate hydrogel films", *Carbohydrate Polymers*, Vol. 98 No. 1, pp. 311-320.

Corresponding author

Paulo Bártolo can be contacted at: paulojorge.dasilvabartolo@manchester.ac.uk